

Article

Experimental Evaluation of the Heat Balance of an Interactive Glass Wall in A Heating Season

Jerzy Szyszka 

Faculty of Civil and Environmental Engineering and Architecture, Rzeszow University of Technology,
35-959 Rzeszów, Poland; jszyszka@prz.edu.pl

Received: 23 December 2019; Accepted: 31 January 2020; Published: 3 February 2020



Abstract: The paper presents an evaluation of the energy efficiency of an interactive glass wall (IGW) prototype. It is a design analogous to Trombe wall. It is capable of giving out the solar radiation heat gains after the sunset. It responds interactively to solar exposure and temperature conditions, regulating the thermal resistance adequately to the requirements. The evaluation of the efficiency of the IGW was based on the analysis of density of heat flux measured on the inner surface of the wall. The experiments were conducted in field conditions using a test chamber of regulated air temperature. The identified parameters of solar energy losses and efficiency enable the IGW heat balance in a heating season in selected climatic conditions to be predicted. In the present paper the IGW heat balance is calculated for the climate in Poland. The calculations proved that the gains of the heat absorbed from solar radiation wall outweigh the losses.

Keywords: interactive glass wall; evaluation of heat balance; transparent intelligent solar active wall; Trombe wall

1. Introduction

The construction industry is responsible for the largest portion of the consumption of energy produced in the world. The predominant part of this amount is used for heating of buildings to ensure an adequate air temperature level. The activities aimed at the reduction of energy consumption are focused on protecting buildings against excessive heat losses. For this purpose, materials and technologies improving the thermal resistance of building exterior envelopes. These include advanced vacuum and electrochromic glazing [1,2], or new generation thermal insulation materials: VIP or nanotechnology based aerogel [3,4]. A considerable potential is demonstrated by the technologies based on the application of building management systems or the so-called intelligent systems that enable the building envelope characteristics to be adapted to changing weather conditions. The heat balance can also be improved by geothermal heat exchangers or recuperators recovering the heat from ventilation air or treated sewage [5]. A natural trend in limiting the energy demand for heat generation is to develop photothermal conversion of solar energy-based systems integrated with the building envelope. In view of ecology and economy, passive or semi-passive systems have a significant potential. Among these, walls that are capable of recovery of heat generated by photothermal conversion of solar energy are in increasing demand. The exterior glazing used for their construction enables solar radiation absorption thus restricting the heat flow transfer to the outdoor surroundings. These design strategies are called Trombe wall (TW) and have been described extensively in specialized literature [6–8]. The energy efficiency of Trombe walls is determined by, inter alia, the physical properties of the materials for their construction and the climatic conditions in which they function as well as the manner they are used [9]. In the classic design, the so-called ventilated wall (Figure 1a) heat is distributed inside the building by means of a mass heating wall owing to heat transfer and as a result of air circulation through the vents in the wall's bottom and top. This solution is highly efficient in solar radiation conversion into heat.

However, its thermal resistance is low. The irregular solar radiation and low temperatures in heating season typical of the Central and Eastern Europe pose a risk of heat loss on days of insufficient solar exposure. This problem was noticed in the design proposed in [10,11]. The thermal resistance was improved by placing an insulating polystyrene wall behind the mass wall (Figure 1b). The flow of the heat generated by the solar irradiance was made possible by air circulation between the ventilated air cavity and the adjacent space owing to the vents in the top and bottom parts of the insulating wall. A similar mode of heat distribution with the circulating air was employed in the wall proposed in [12]. In this case, the thermal insulating layer directly behind the selective absorber (Figure 1c). Based on the experiments performed in the climate of the Qinghai province in China, the authors proved that the efficiency of heat gains utilisation, calculated as the ratio between the heat entering a building and the sum of solar irradiance reaching the wall surface increased by 56% compared with the classic Trombe wall operating in identical conditions. In [13] a hybrid heat collecting facade (HHCF) was proposed, which can reduce the heating demand by 40.2% and 21.5% compared with the conventional direct solar heat gain window and the Trombe Wall.

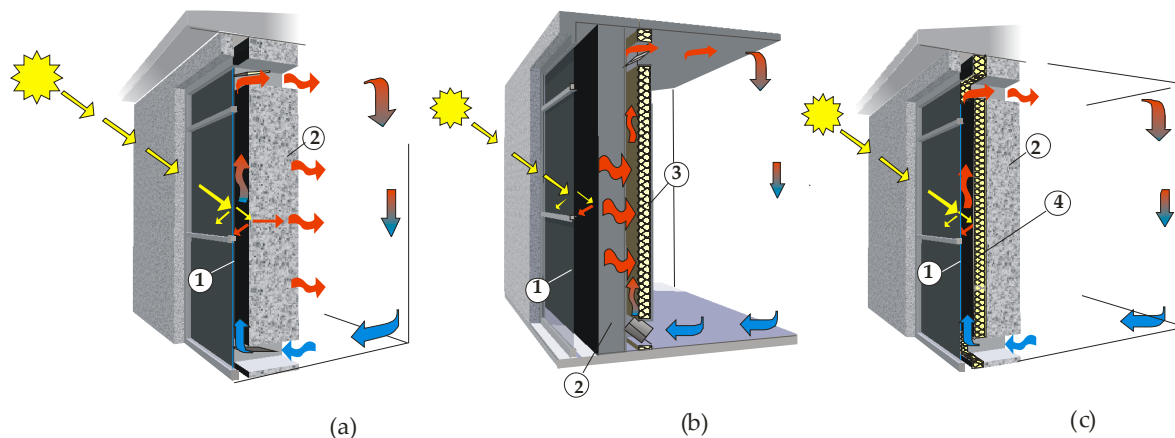


Figure 1. Thermal operation of passive walls: (a) classic Trombe wall, (b) composite Trombe wall with an insulating panel, (c) composite Trombe wall with a selective absorber. 1—glazing, 2—massive wall, 3—insulating polystyrene wall, 4—insulating layer directly behind the selective absorber.

Along with the studies on the improvement of TW thermal efficiency, modification proposals are formulated to improve their performance. The examples include a TWPV integrated with photovoltaic cells [14–16], a hybrid system composed of a phase change materials-ventilated Trombe wall (PCMs-VTW) [17] or A thermal-catalytic (TC) Trombe wall with a capacity for the reduction of air formaldehydes [18]. Transparency may be one of the desirable functions of the thermal wall. Water walls have this property while preserving the potential for heat absorption and storage. In the design discussed in [19] a mass heating wall was replaced with a glass container filled with water safeguarded against algae growth. To intensify solar absorption the water was coloured and special light diffusing inserts were placed in the container (Figure 2).

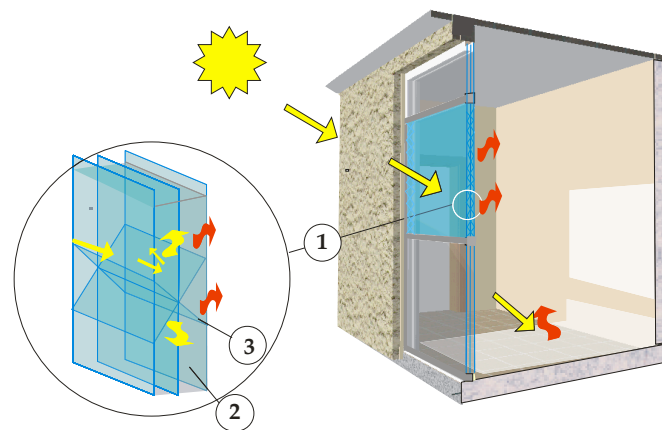


Figure 2. Water Trombe wall (transwall): 1—glass water container, 2—colored water, 3—diffusing-absorbing inserts.

Another type of a transparent wall capable of interactive response to weather conditions is the design of the IGW presented in the paper (Figure 3). Because of its capacity for solar radiation conversion and potential for solar gains generation, even after the sunset, it is a wall analogous to the Trombe wall. The wall's interactivity and corresponding selective thermal resistance result in solar irradiance intensification and heat loss reduction in periods of insufficient solar irradiance.

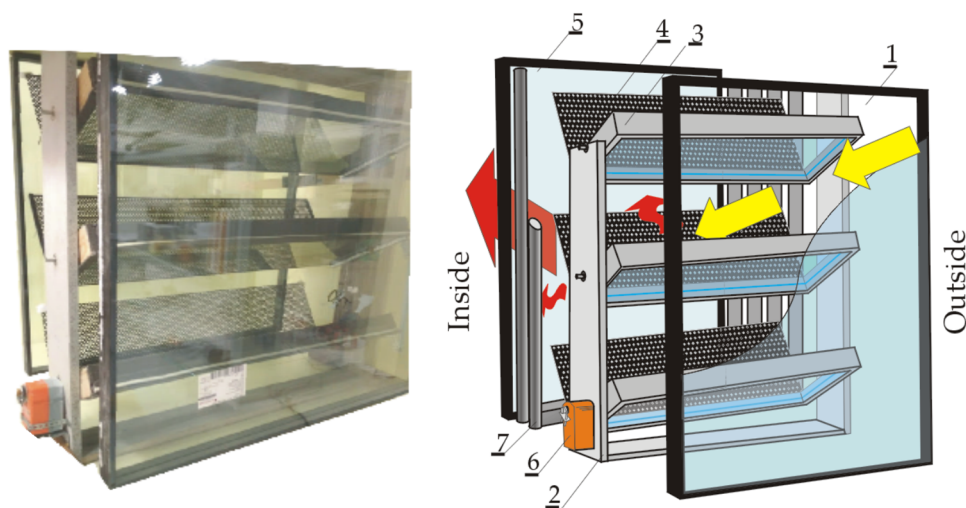


Figure 3. The prototype of the tested interactive glass wall (IGW): 1—outer glazing, 2—louvers headrail, 3—swivelling louvers panels, 4—moveable absorber, 5—interior glazing, 6—louvers panels swivelling actuator, 7—containers with heat storing materials.

IGW was designed as an alternative to nonbearing panel walls. According to the requirements or an architectonic vision, it can be used to fill in completely or partially the space between the structural elements. In the evaluation of the thermal efficiency of passive systems numerical models based on the finite element method or the method of finite differences are often employed [20–24]. They offer the possibility of very accurate mapping of the model's thermal performance, which is confirmed by experiment-based validation [25]. However, they require highly specialized knowledge of numerical modelling, building physics and thermodynamics. In the evaluation of the thermal efficiency of prototypes the validation of numerical models is strongly supported by the data obtained from experimental tests performed on physical models in natural [26] or laboratory conditions [27]. The evaluation of the thermal efficiency of the IGW presented in the paper was based on the analysis of the data obtained in the field tests on the IGW using a test chamber of controlled indoor temperature.

2. IGW Prototype Design and Test Method

This section is devoted to the details of the IGW prototype design and the test stand. The adopted method, based on experimental tests, of the determination of the specific parameters of the IGW prototype heat balance components is discussed.

2.1. Description of the Tested Prototype

The prototype of a wall element IGW (Figure 4) was made from three triple glazed units each of overall heat transfer coefficient of $U_g = 0.5 \text{ W/m}^2\text{K}$ (gain factor $g = 0.55$, emissivity $e = 0.92$). To facilitate the solar radiation access inside the components and intensify heat transfer to the building, the central unit was made in the louver window technology. The absorbers made of perforated black sheet (absorption coefficient $\alpha = 0.95$) were attached to the swivelling louver panels so that, after swivelling the panels, the absorber was exposed as vertically to the sunlight rays as possible. The operation of the glass panels swivelling was made automatic by connecting the actuator that regulates the swivelling with a controller responding to air temperature and solar irradiance I_g measured in the space between the glazed units. The threshold values were adopted at $20 \text{ }^\circ\text{C}$ for the temperature T_1 of the air in the space between the glazed units and 50 W/m^2 for the solar irradiance I_g measured behind the outer glazing.

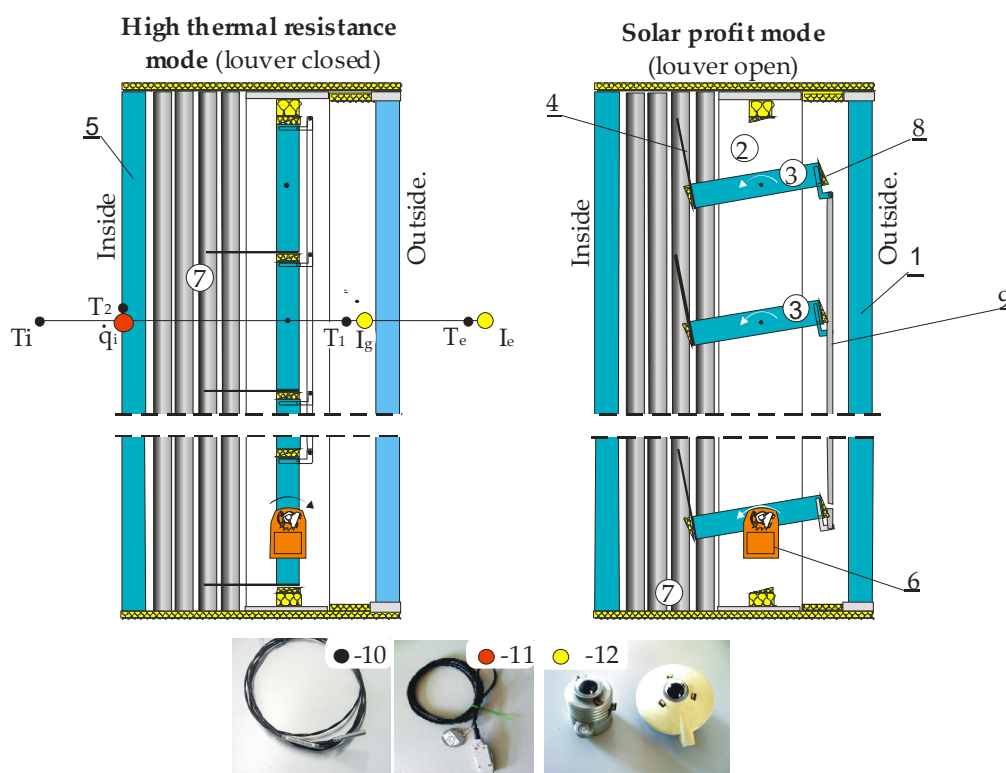


Figure 4. The prototype of the tested wall: 1—exterior glazing, 2—louvers headrail, 3—swivelling louvers panels, 4—moveable absorber, 5—interior glazing, 6—louvers panels swivelling actuator, 7—containers with heat storing materials containers, 8—aerogel mat seal, 9—relay rods, 10—temperature sensors, 11—density heat flux sensor, 12—pyranometers.

The storage of the heat absorbed inside an IGW was made possible by the containers placed on the sides, filled with phase change materials of the total weight of 5.55 kg. Rubitherm GmbH manufactured commercial phase change material RT 28, with the value of enthalpy of fusion and solidification interval of $\Delta H_{fus} = 220\text{--}225 \text{ J/g}$, m.p. = $28 \text{ }^\circ\text{C}$ and solidification temperature = $21 \text{ }^\circ\text{C}$ was used.

2.2. Description of Test Stand

The energy efficiency of IGW was evaluated on the basis of the results obtained in a test chamber with regulated indoor air temperature T_i in field conditions. The prototype of the IGW of dimensions 890×885 mm was installed in a facing south wall of the test chamber (Figure 5). It was thermally separated from the wall in which it was fixed by means of extruded polystyrene layer 0.08 m thick and polyurethane foam.

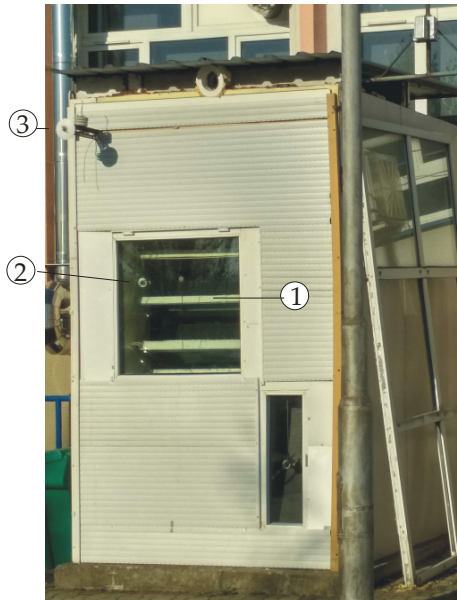


Figure 5. The chamber for field tests: 1—IGW module, 2—pyranometer (I_g) placed behind the exterior glazing, 3—pyranometer (I_e) placed outside the chamber.

In the chamber the air temperature was stabilized at the level of 20 °C. The tested parameters were recorded by heat flow density sensors ALMEMO FQ A020 C and temperature sensors PT1000 as well as pyranometers Delta OHM LPPYRA03AC (sensitivity 10 mV/(kW/m²) interacting with 16 Channel Data Acquisition Monitoring System Comet MS6D. The arrangement of the sensors is shown in Figures 4 and 6. The data were recorded with the frequency of every five minutes. The louver was controlled by MP018 Relays Module Output interacting with the Comet recorder. List of the employed apparatus and sensors together with their measurement accuracy has been listed in Table 1.

Table 1. Measurement accuracy of employed sensors and Data Acquisition Monitoring System.

Kind of Sensor	Type of Sensor	Accuracy
Temperature sensor	PT1000	A class (<0.2 °C)
Irradiation sensor	DeltaOhm LP Pyra12	<1 % (first class)
Heat flow density	DeltaOhm LPPyra03	$<\pm 0.2\%$ (second class)
	ALMEMO FQ A020 C	$<6\%$ of measured value
	Comet MS6D 16 Channel Data Acquisition Monitoring System	
DC	4 to 20 mA	$\pm 0.1\%$ (± 0.02 mA)
DC	-10 V to $+10$ V	$\pm 0.1\%$ (± 10 mV)
Temperature	PT1000	± 0.2 °C (-200 °C to $+100$ °C)

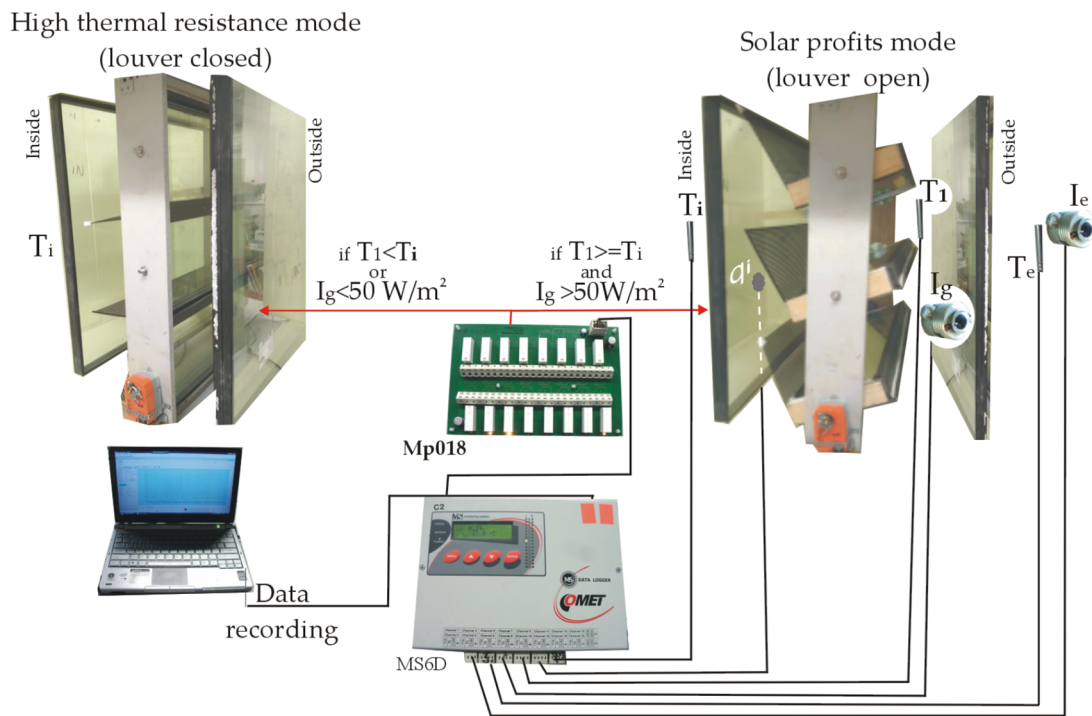


Figure 6. Measuring and control system diagram.

The tests were conducted in winter 2018/2019 in Rzeszów, Poland (50°02'01"N, 22°00'17"E).

2.3. Description of the Method for the Evaluation of IGW Thermal Efficiency

The parameter of IGW thermal efficiency evaluation that can be adopted as measurable is the wall’s heat balance. The energy state of the wall separating the indoor environment from the outdoor environment of a building can be measured by, inter alia, the density of heat flow rate q_i taken at, for instance, its inner surface. It is a resultant of the flow connected with heat loss q_H , and the flow coming from solar radiation q_S :

$$q_i = f(q_H, q_S) \tag{1}$$

The heat balance of the wall in time interval of $\langle t1:t2 \rangle$ is expressed by equation:

$$Q = A \cdot \int_{t1}^{t2} q_i dt = A \cdot \int_{t1}^{t2} (q_H - q_S) dt \tag{2}$$

The value of the flow of loss q_H is determined by the wall thermal resistance R_{IGW} and difference between the temperature of air on its sides:

$$q_H = \frac{\Delta T}{R_{IGW}} = U_{IGW_EMP} \cdot \Delta T, \tag{3}$$

where:

- R_{IGW} —total thermal resistance of IGW ((m²·K)/W),
- U_{IGW} —heat transfer coefficient of IGW (W/(m²·K)),
- ΔT —temperature difference on the wall’s sides.

In the case of heat flow density measurement in the conditions of steady state heat flow or a quasi steady state which is accompanied by minor temperature fluctuations at negligibly small solar

irradiance, using Equations (2) and (3) the empirical coefficient of heat transfer U_{IGW_EMP} can be determined:

$$U_{IGW_EMP} = \frac{\bar{q}_i}{\Delta T} \quad (4)$$

On the basis of the dependencies above also solar gains can be evaluated. The solar gains related heat flow q_s is determined by solar irradiance and the properties of the wall in the aspect of heat transfer indoor. A significant amount of the absorbed heat is lost as an effect of additional losses resulting from the increase of the wall temperature. The absorption of sunlight after the time necessary for heat flow transfer to the inner surface results in a reduction of flow q_i , from the value q_H (Equation (3)) to a level proportional to the amount of the energy absorbed. Consequently, solar gains Q_S in the time interval of $(t1:t2)$ can be calculated from the equation:

$$Q_S = A \cdot \int_{t1}^{t2} (q_H - q_i) dt, \quad (5)$$

where:

A —total pane area (m^2).

Solar Heat Gain Utilisation (SHGU) efficiency η_{SHGU} referred to the sum of solar irradiance transferred through the outer glazing S_g in IGW balance, can be calculated from the equation:

$$\eta_{SHGU}(I_g) = \frac{A \cdot \int_{t1}^{t2} (q_H - q_i) dt}{c_g \cdot A \cdot \int_{t1}^{t2} I_g dt} \cdot 100\% = \frac{Q_S}{S_g} \cdot 100\% \quad (6)$$

where:

C_g —ratio of the outer glazing visible area (not covered by the glazing bead) to the total glazing inner area IGW ($C_g = 0.89$),

S_g —the sum of solar irradiance transferred through the outer glazing (Wh/m^2).

3. Results and Discussion

In this section, based on the experimental data, the specific parameters of IGW heat balance components are determined. The method was validated. Using the determined parameters and the climate data of a typical meteorological year the IGW heat balance was calculated for a heating season of a selected locality, which was followed by a discussion of the results.

From the results recorded at the turn of November and December the period of low radiation and a period determined by heat gains from high irradiation period were selected (Figure 7) On the basis of heat flux density distribution on IGW indoor surface at minor temperature variations at low solar irradiance an empirical value of heat transfer coefficient U_{IGW_EMP} was determined.

In the periods of high radiation during the day the temperature variations were large. During the day the temperature of air heated by the sun increased. At night-time, with no cloud cover, the radiation heat exchange with the sky increased the temperature drop.

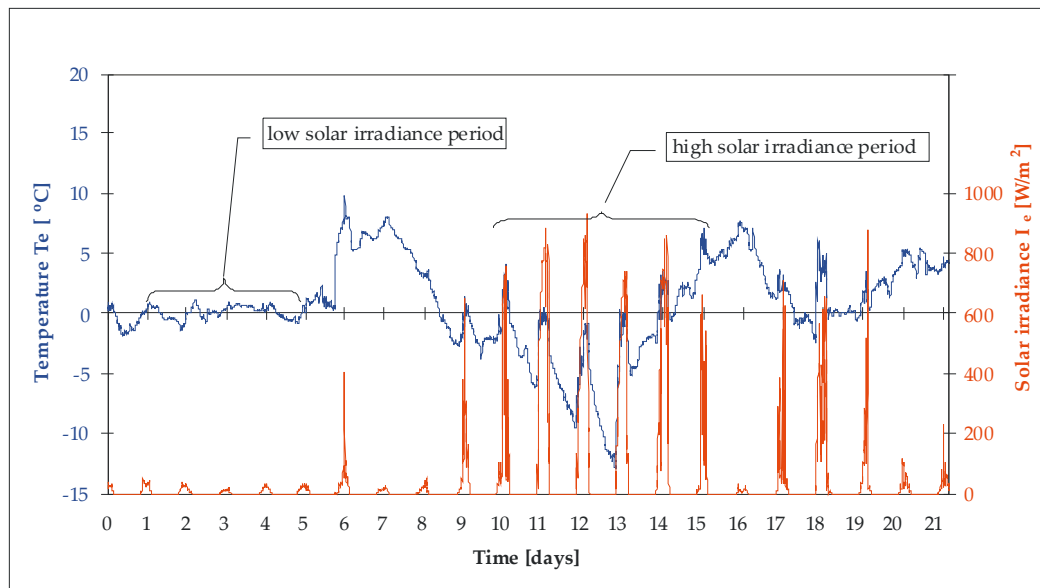


Figure 7. Air temperature distribution vs. solar irradiance recorded outside the test chamber in analyzed period.

3.1. Empirical Heat Transfer Coefficient U_{IGW}

IGW can operate in two modes. In one, the “high thermal resistance” the closed inner louver ensures maximum thermal resistance. In the other one, the “solar profit mode” opening the louvers enables more efficient heating of IGW interior as a result of reduced thermal resistance. To determine the empirical values of the heat transfer coefficients in both modes, from the recorded data the days were selected on which low solar irradiance was accompanied by minor fluctuations of outdoor air temperature. In the period between November 2018 and mid-February 2019 the wall operated in the interactive mode. Using the data from this period the empirical heat transfer coefficient $U(R_{max})$ corresponding to the maximum thermal resistance of IGW was identified (Figure 8, Table 1). From the turn of February and March 2019 tests were conducted with the blocked open inner louver. From this period data that were used for the identification of heat transfer coefficient $U(R_{min})$ corresponding to a reduced value of thermal resistance of IGW were selected (Table 2).

Table 2. Averaged daily values of heat flux density, outdoor temperature and empirically determined heat transfer coefficient.

Number of Day	$\bar{q}_i [\frac{W}{m^2}]$	$\overline{\Delta T} [^{\circ}K]$	$\bar{U}_{EMP}(R_{max}) [\frac{W}{m^2K}]$
1	3.409	20.70	0.165
2	3.685	20.67	0.178
3	3.425	20.12	0.170
4	3.375	20.16	0.167
5	3.242	20.02	0.162
	Mean value \bar{x}		0.168
	Standard deviation $\sqrt{\frac{\sum(x-\bar{x})^2}{(n-1)}}$		0.006

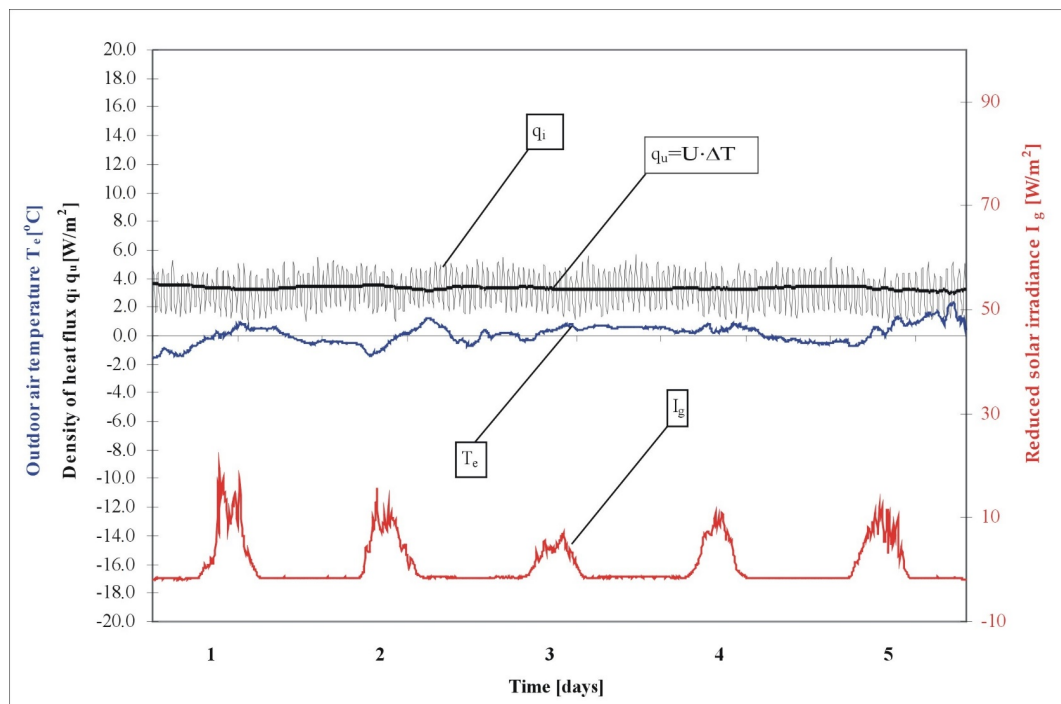


Figure 8. Distribution of outdoor air temperature (T_e), heat flux density measured on the inner surface of the IGW and solar irradiance measured behind the outer glazing in the very low radiation period.

Finally, on the basis of the results (Tables 2 and 3) the IGW heat transfer coefficient was described with Equation (7):

$$U_{IGW_EMP} = \left\{ \begin{array}{l} 0.255 \text{ if } T_1 > 20^\circ \text{C and } I_g > 50 \frac{\text{W}}{\text{m}^2} \\ 0.168 \text{ in other cases} \end{array} \right\}, \quad (7)$$

With the known heat transfer coefficient, it is possible to predict the heat flux component $q_{H(U)}$ connected with the heat loss proportional to air temperature difference ΔT on both sides of the wall, which can be expressed with a formula (Equation (8)).

$$q_{H(U)} = \bar{U}_{EMP} \cdot \Delta \bar{T} = \left\{ \begin{array}{l} 0.255 \text{ if } T_1 > 20^\circ \text{C and } I_q > 50 \frac{\text{W}}{\text{m}^2} \\ 0.168 \text{ in other cases} \end{array} \right\} \cdot \Delta \bar{T}, \quad (8)$$

Table 3. Averaged daily values of heat flux density, outdoor air temperature and empirically determined heat transfer coefficient in “solar profit” mode.

Number of Day	$\bar{q}_i [\frac{\text{W}}{\text{m}^2}]$	$\Delta \bar{T} [^\circ \text{K}]$	$\bar{U}_{EMP}(R_{\min}) [\frac{\text{W}}{\text{m}^2 \text{K}}]$
1	5.08	20.14	0.252
2	5.05	20.45	0.247
3	5.38	20.23	0.266
	Mean value \bar{x}		0.255
	Standard deviation $\sqrt{\frac{\sum (x-\bar{x})^2}{(n-1)}}$		0.01

3.2. Determination of the Solar Heat Gain Utilisation Efficiency (η_{SHGU})

The impact of solar irradiance on IGW results in the reduction of the heat flux density. Depending on the irradiance, the resultant heat flux may reach a negative value, which indicates heat transfer to the building interior. The comparison of the real flux q_i with flux q_u calculated after Equation (7) for air temperature difference ΔT on both sides of the wall in a given time interval was a basis for the

calculation of the actual solar gains Q_S . The knowledge of solar gains referred to the sum of solar irradiance that generated these gains enables the estimation of the solar heat gain utilisation efficiency η_{SHGU} in IGW (Equation (6)). The efficiency referred to the sum of solar irradiance transferred through the outer glazing S_g , is expressed by the equation:

$$\eta_{SHGU}(I_g) = \frac{Q_S}{S_g} \cdot 100\% = \frac{A \cdot \int_{t1}^{t2} (q_{H(U)} - q_i) dt}{c_g \cdot A \cdot \int_{t1}^{t2} I_g dt} \cdot 100\%, \tag{9}$$

where:

$I_g [\frac{W}{m^2}]$ —solar irradiance transferred through the outer glazing in time interval ($t1:t2$).

To determine efficiency η_{SHGU} using the dependencies described by Equations (8) and (9) the period of high sums of daily solar irradiation was selected (Figure 9).

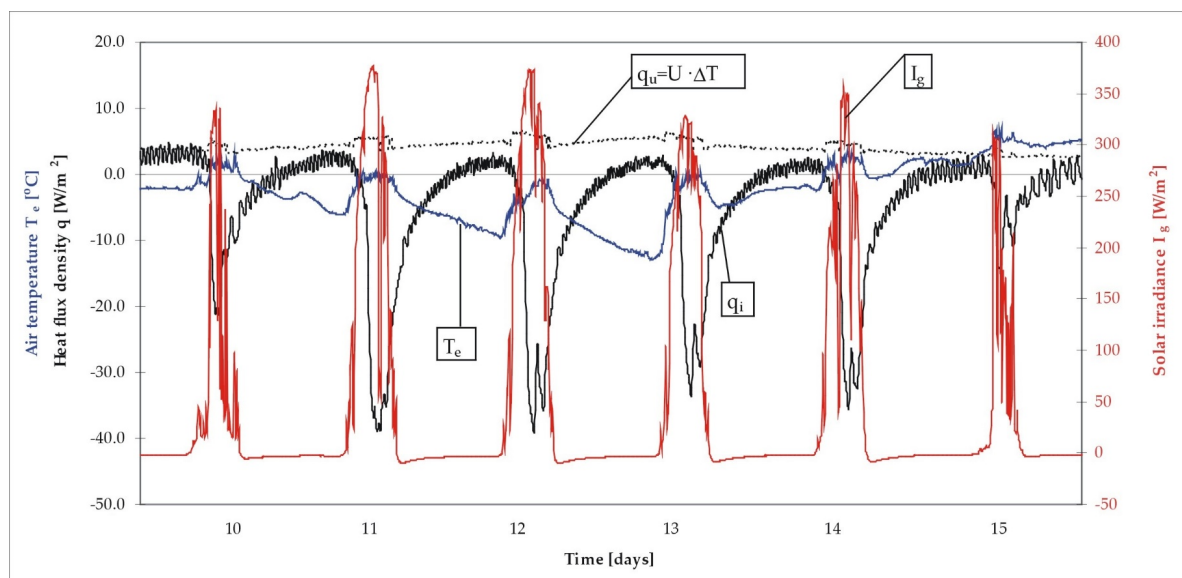


Figure 9. Distribution of air temperature outside the chamber T_e , heat flux density measured on the IGW inner surface and solar irradiance measured behind the glazing in the period of considerable solar radiation.

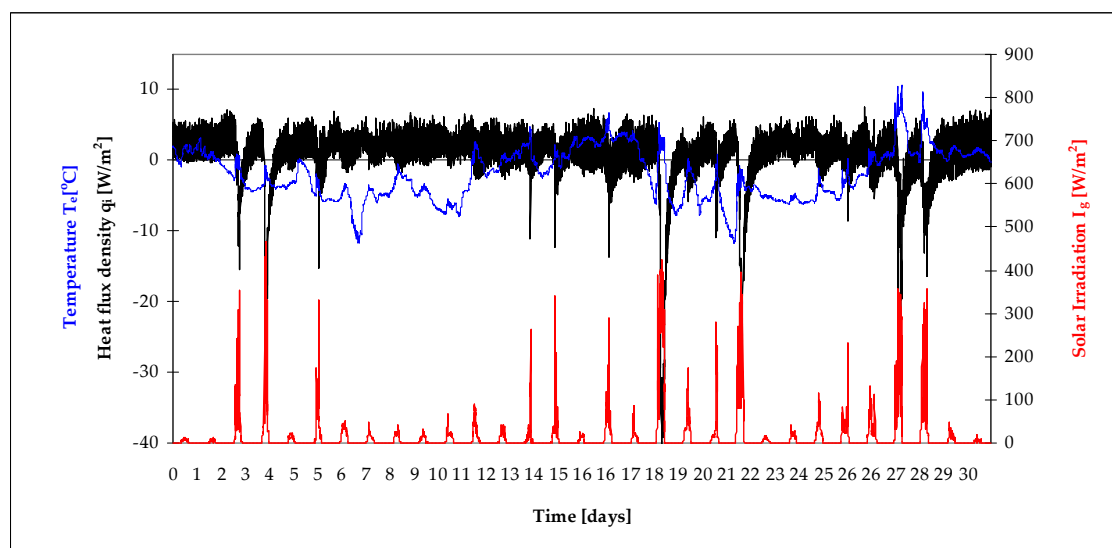
Solar heat gain utilisation efficiency η_{SHGU} in IGW calculated from Equation (9) and its components are tabulated in Table 4.

Table 4. Daily sums of solar gains Q_s , solar irradiance measured behind the outer glazing of IGW and calculated efficiency η_{SHGU} .

Number of Day [n]	Q_s [$\frac{Wh}{m^2}$]	S_g [$\frac{Wh}{m^2}$]	η_{SHGU}
10	131.61	608.1	21.64
11	276.60	1440.8	19.20
12	289.75	1398.1	20.73
13	249.51	1190.6	20.96
14	236.32	1143.3	20.67
15	104.56	438.6	23.84
Mean value \bar{x}			21.17
Standard deviation $\sqrt{\frac{\sum (x-\bar{x})^2}{(n-1)}}$			1.53

3.3. Validation of IGW Heat Balance Calculation Mode

For the validation of the possibility of the IGW heat balance prediction the results recorded in the period of 1–31 January 2019 (Figure 10) were chosen. The wall's heat balance calculated on the basis of the recorded heat flux density on the inner surface IGW $Q(q_i)$ was compared with the balance calculated on the basis of the determined heat transfer coefficient U_{IGH} and the efficiency of solar energy utilisation η_{SHGU} .

**Figure 10.** Distribution of air temperature T_e , heat flux density measured on the inner surface of the IGW and solar irradiation measured behind the outer glazing in January 2019.

The validation study was based on the comparison of IGW heat balance calculation based on the heat flux density recorded in the period of 1–31 January 2019 on the inner surface Q_i (Equation (2)) with the balance Q_H calculation based on heat transfer coefficient U_{IGW} (Equations (7) and (8)), and the solar gain Q_s calculation based on solar heat gain utilisation efficiency η_{SHGU} in IGW (Equation (9)) referred to the sum of solar radiation recorded behind the glazing. The calculation results are tabulated in Table 5.

Table 5. Heat balance components calculated for January 2019.

$Q_i = A \cdot \int q_i dt$	$Q_H = A \cdot \int q_{H(U)} dt$	$Q_S = \eta_{SHGU} \cdot c_g \cdot A \cdot \int I_g dt$	$Q_H - Q_S$	$\Delta Q = \frac{Q_i - (Q_H - Q_S)}{Q_i} \cdot 100\%$
575.89 [Wh]	3084.79 [Wh]	2419.46 [Wh]	665.33 [Wh]	15.53%

From the tabulated results it can be concluded that the difference ΔQ between the balance determined from the heat flux density measured on the IGW inner surface and the balance calculated on the basis of heat transfer coefficient U_{IGW} and solar heat gain utilisation efficiency η_{SHGU} is 15.53%. This difference indicates that either the solar gains component is underestimated or the heat loss component overestimated. In the context of the calculations of the potential solar irradiation derived heat gains the difference is on the margin of calculations safety.

3.4. Prediction of IGW Heat Balance in a Heating Season Based on Climate Database

To predict IGW balance the database of 30-year observation based typical meteorological years, available on website of the Ministry of Digitisation RP was used data [28]. It had been developed for the necessary calculations of energy consumption/generation in the construction industry. It can be used for the calculation of energy characteristics of buildings and issuing energy certificates for buildings, in energy auditing as well as the design and energy simulation of buildings. Balance calculations (Equation (10)) were performed in a calculation spreadsheet with hourly temperatures of outdoor air and hourly sums of solar radiation striking the surface vertical to the meteorological station proper for the city of Rzeszów. The calculations were done for South (S), South-East (S-E), South-West (S-W), East (E) and West (W) orientations of the IGW in the months of October to April.

$$Q = A \cdot \sum U_{IGW_EMP} \cdot (T_i - T_e) - A \cdot g \cdot \eta_{SHGU} \cdot C_g \cdot \sum S_{eh}, \quad (10)$$

where:

A —surface of IGW (1 m²),

U_{IGW} —heat transfer coefficient (after Equation (7)),

T_i —indoor air temperature ($T_i = 20$ °C)],

S_{eh} —hourly sum of solar irradiation recorded in front of the glazing,

g —gain factor ($g = 0.55$ according to the manufacturer's specifications of the glazing used).

Based on the g value, sum of solar irradiation behind the outer glazing S_{gh} can be determined:

$$S_{eg} = S_{eh} \cdot g, \quad (11)$$

The results of the calculations of heat balance per the area of 1 m² in each month of the heating season are tabulated in Table 6 and Figure 11. The Negative values indicate the overbalance of heat gains over losses.

Table 6. Heat balance calculated for the months of the heating season depending on the orientation with respect to cardinal points.

Month	Heat Balance [Wh/m ²]				
	E	SE	S	SW	W
October	-2442.03	-3526.65	-4226.97	-3592.03	-2492.84
November	42.10	-993.54	-1691.16	-1240.25	-132.42
December	835.30	-237.27	-841.21	-390.31	727.05
January	764.06	-571.02	-1160.47	-421.21	870.04
February	-884.79	-2124.54	-2690.94	-1839.41	-692.03
March	-3260.19	-4298.28	-4679.78	-3861.34	-2921.9
April	-6536.78	-7243.21	-7272.98	-6953.11	-6259.6

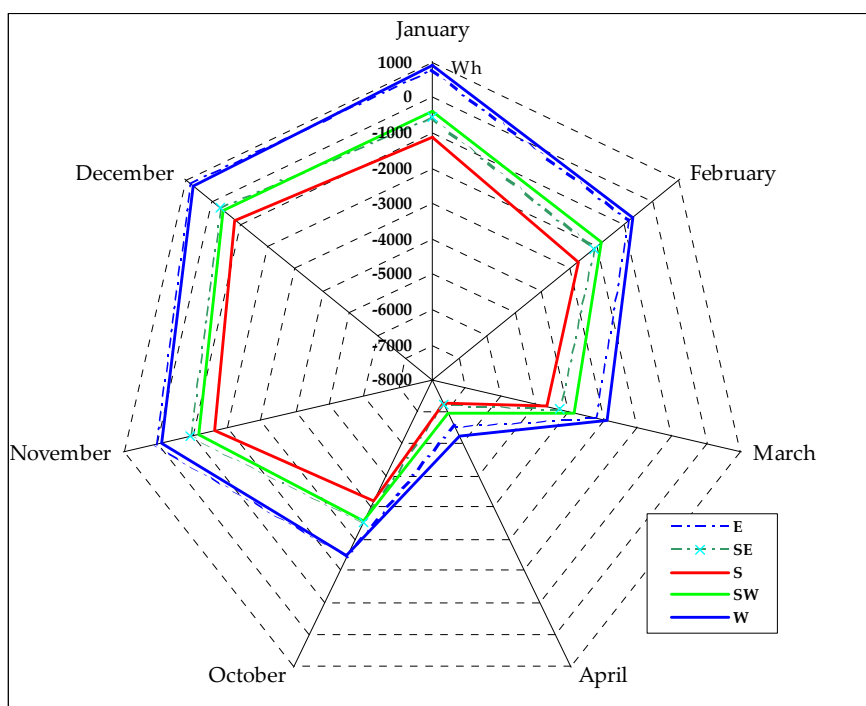


Figure 11. Heat balance calculated for the months of the heating season depending on the orientation with respect to cardinal points chart.

What is noticeable in the presented results is the overbalance of the irradiation derived gains over losses in each month of the heating season in the wall oriented towards south-east, south and south-west. The solar irradiation of the eastern and western orientation did not compensate for the heat loss in the period November–January. Considering the fact that the proposed method of balance estimation is biased with ca. 15.5% margin of heat gains underestimation, the results can be regarded as satisfactory with respect of calculations safety. The target of the IGW design optimization was not the maximization of gains but instead its functionality related to its transparency properties. Unlike typical windows, the IGW heat thermal capacitance enables the irradiation derived gains to be transferred also to the time after the sunset. This property is illustrated in the diagram in Figure 12.

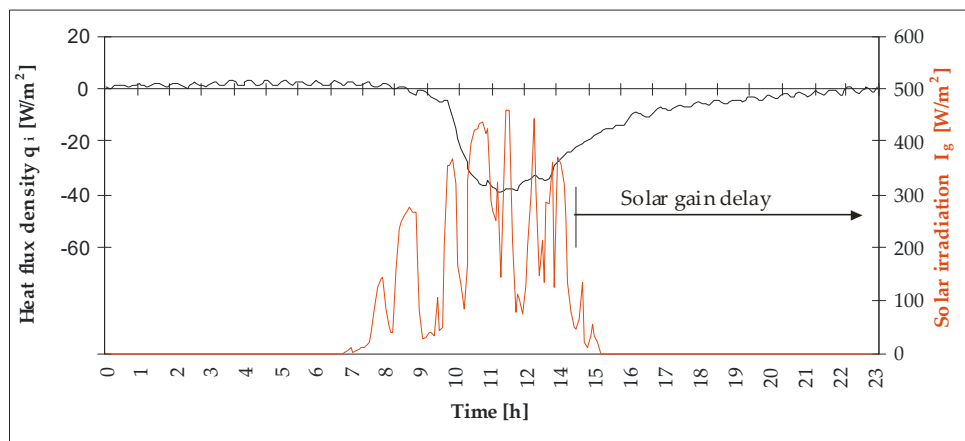


Figure 12. An example of heat flux density distribution on the IGW inner surface during a day.

Depending on the daily sum of solar radiation the IGW inner surface generates a flux oriented towards the building interior even eight hours after the sunset. It should also be noted that the heat flux given up by the wall surface during the day did not exceed 40 W/m^2 . It is a value ten times lower than the solar radiation transferred through the outer glazing. This property is significant for the occupants' comfort.

4. Conclusions

The present paper is devoted to the evaluation of the energy efficiency of an interactive wall responding to changing conditions of solar radiation and air temperature proposed by the author. Following the analysis of the results of field experimental tests conducted using a physical model the parameters characterising the heat balance components were determined. They were employed in the simplified method of IGW heat balance prediction on the basis of weather data of a typical meteorological year. A number of final conclusions were formulated.

- (1) The prediction of heat balance calculated for a heating season for a selected locality indicated the overbalance of heat gains over losses in all the months of the season when the IGW was oriented to the south, south-east and south-west. The western and eastern orientations in November and December resulted in the predominance of heat losses.
- (2) The tests indicated that, unlike conventional windows, apart from transparency, owing to the use of phase-change materials (PCM) in the IGW structure, it has the capacity of giving up heat gains even eight hours after the sunset.
- (3) The test results confirm the potential of the interactive designs, which apart from transparency, have the capacity to reduce the conventional energy demand and exert a favourable impact on the functionality of a building and occupants' comfort. The use of cutting-edge technologies and their increasing availability for the shaping of the outer envelope of a building opens up new possibilities of construction engineering.
- (4) The validity of the method discussed in the paper indicated a difference in the heat balance calculated on the basis of the recorded heat flux density at the level of 15.53% of heat gains underestimation or its losses overestimation, which can be considered a result satisfactory with respect of calculations safety.

The heat characteristics of IGW, the validation of heat balance prediction method based on experimentally identified U_{EMP} and η_{USRH} presented in the paper should be regarded as one of the stages of the research. Further research is planned on a greater scale, in which special attention will be focused on the improvement of the thermal capacitance and optimization of glazing selection in order to increase heat gains and the capacity of their storage.

5. Patents

Szyszkza, J., Rzeszow University of Technology, A collector-accumulative transparent wall for construction engineering; Patent application 12.04.2018 r. nr P.425203 PL.

Funding: This research received no external funding.

Acknowledgments: The author would like to thank Prof. Lech Lichołai making available the infrastructure and equipment necessary to conduct the tests.

Conflicts of Interest: The author declares no conflict of interest. The funders had no role in the design of the study; in the collection, analyses, or interpretation of data; in the writing of the manuscript, or in the decision to publish the results.

References

- Kim, S.-C.; Yoon, J.-H.; Lee, R.-D. Energy Performance Assessment of a 2nd-Generation Vacuum Double Glazing Depending on Vacuum Layer Position and Building Type in South Korea. *Energies* **2017**, *10*, 1240.
- Al Dakheel, J.; Tabet Aoul, K. Building Applications, Opportunities and Challenges of Active Shading Systems: A State-of-the-Art Review. *Energies* **2017**, *10*, 1672. [[CrossRef](#)]
- Biswas, K.; Jogineedi, R.; Desjarlais, A. Experimental and Numerical Examination of Naturally-Aged Foam-VIP Composites. *Energies* **2019**, *12*, 2539. [[CrossRef](#)]
- Buratti, C.; Moretti, E.; Zinzi, M. High Energy-Efficient Windows with Silica Aerogel for Building Refurbishment: Experimental Characterization and Preliminary Simulations in Different Climate Conditions. *Buildings* **2017**, *7*, 8. [[CrossRef](#)]
- Sohail, U.; Kwiatek, C.; Fung, A.S.; Joksimovic, D. Techno-Economic Feasibility of Wastewater Heat Recovery for A Large Hospital in Toronto, Canada. *Multidiscip. Digit. Publ. Inst. Proc.* **2019**, *23*, 1. [[CrossRef](#)]
- Saadatian, O.; Sopian, K.; Lim, C.H.; Asim, N.; Sulaiman, M.Y. Trombe walls: A review of opportunities and challenges in research and development. *Renew. Sustain. Energy Rev.* **2012**, *16*, 6340. [[CrossRef](#)]
- Zhongting, H.; Wei, H.; Jie, J.; Shengyao, Z. A review on the application of Trombe wall system in buildings. *Renew. Sustain. Energy Rev.* **2017**, *70*, 976–987.
- Zhang, H.; Shu, H.J. A Comprehensive Evaluation on Energy, Economic and Environmental Performance of the Trombe Wall during the Heating Season. *J. Therm. Sci.* **2019**, *28*, 1141–1149. [[CrossRef](#)]
- Bevilacqua, P.; Benevento, F.; Bruno, R.; Arcuri, N. Are Trombe walls suitable passive systems for the reduction of the yearly building energy requirements? *Energy* **2019**, *185*, 554–566. [[CrossRef](#)]
- Zalewski, L.; Chantant, M.; Lassue, S.; Duthoit, B. Experimental thermal study of a solar wall of composite type. *Energy Build.* **1997**, *25*, 7–18. [[CrossRef](#)]
- Shen, J.; Lassue, S.; Zalewski, L.; Huang, D. Numerical study on thermal behavior of classical or composite Trombe solar walls. *Energy Build.* **2007**, *39*, 962–974. [[CrossRef](#)]
- Ji, J.; Luo, C.; Sun, W.; Yu, H.; He, W.; Pei, G. An improved approach for the application of Trombe wall system to building construction with selective thermo-insulation façades. *Chin. Sci. Bull.* **2009**, *54*, 1949. [[CrossRef](#)]
- Wang, X.; Lei, B.; Bi, H.; Yu, T. Study on the Thermal Performance of a Hybrid Heat Collecting Facade Used for Passive Solar Buildings in Cold Region. *Energies* **2019**, *12*, 1038. [[CrossRef](#)]
- Hu, Z.; He, W.; Ji, J.; Hu, D.; Lv, S.; Chen, H.; Shen, Z. Comparative study on the annual performance of three types of building integrated photovoltaic (BIPV) Trombe wall system. *Appl. Energy* **2017**, *194*, 81–93. [[CrossRef](#)]
- Lin, Y.; Ji, J.; Zhou, F.; Ma, Y.; Luo, K.; Lu, X. Experimental and numerical study on the performance of a built-middle PV Trombe wall system. *Energy Build.* **2019**, *200*, 47–57. [[CrossRef](#)]
- Irshad, K.; Habib, K.; Thirumalaiswamy, N. Performance Evaluation of PV-trombe Wall for Sustainable Building Development. *Procedia CIRP* **2015**, *26*, 624–629. [[CrossRef](#)]
- Liu, X.; Zhou, Y.; Li, C.-Q.; Lin, Y.; Yang, W.; Zhang, G. Optimization of a New Phase Change Material Integrated Photovoltaic/Thermal Panel with The Active Cooling Technique Using Taguchi Method. *Energies* **2019**, *12*, 1022. [[CrossRef](#)]
- Yu, B.; Jiang, Q.; He, W.; Hu, Z.; Chen, H.; Ji, J.; Xu, G. The performance analysis of a novel TC-Trombe wall system in heating seasons. *Energy Convers. Manag.* **2018**, *164*, 242–261. [[CrossRef](#)]

19. Nayak, J.K. Transwall versus trombe wall: Relative performance studies. *Energy Convers. Manag.* **1987**, *27*, 389–393. [[CrossRef](#)]
20. Li, S.; Zhu, N.; Hu, P.; Lei, F.; Deng, R. Numerical study on thermal performance of PCM Trombe Wall. *Energy Procedia* **2019**, *158*, 2441–2447. [[CrossRef](#)]
21. Corasaniti, S.; Manni, L.; Russo, F.; Gori, F. Numerical simulation of modified Trombe-Michel Walls with exergy and energy analysis. *Int. Commun. Heat Mass Transf.* **2017**, *88*, 269–276. [[CrossRef](#)]
22. Leang, E.; Tittlein, P.; Zalewski, L.; Lassue, S. Numerical study of a composite Trombe solar wall integrating microencapsulated PCM. *Energy Procedia* **2017**, *122*, 1009–1014. [[CrossRef](#)]
23. Simo-Tagne, M.; Ndukwu, M.C.; Zoulalian, A.; Bennamoun, L.; Kifani-Sahban, F.; Rogaume, Y. Numerical analysis and validation of a natural convection mix-mode solar dryer for drying redchilli under variable conditions. *Renew. Energy* **2019**. [[CrossRef](#)]
24. Simo-Tagne, M.; Ndukwu, M.C.; Rogaume, Y. Modelling and numerical simulation of hygrothermal transfer through a building wall for locations subjected to outdoor conditions in Sub-Saharan Africa. *J. Build. Eng.* **2019**, *26*, 100901. [[CrossRef](#)]
25. Barone, G.; Buonomano, A.; Forzano, C.; Palombo, A. Building Energy Performance Analysis: An Experimental Validation of an In-House Dynamic Simulation Tool through a Real Test Room. *Energies* **2019**, *12*, 4107. [[CrossRef](#)]
26. Briga-Sá, A.; Boaventura-Cunha, J.; Lanzinha, J.C.; Paiva, A. An experimental analysis of the Trombe wall temperature fluctuations for high range climate conditions: Influence of ventilation openings and shading devices. *Energy Build.* **2017**. [[CrossRef](#)]
27. Szyszka, J. Simulation of modified Trombe wall. *E3S Web Conf.* **2018**, *49*, 00114. [[CrossRef](#)]
28. Website of the Ministry of Funds and Regional Policy Republic of Poland, Data for A the Typical Meteorological Year for Rzeszow. Available online: <https://www.gov.pl/web/fundusze-regiony/dane-do-obliczen-energetycznych-budynkow> (accessed on 22 June 2019).



© 2020 by the author. Licensee MDPI, Basel, Switzerland. This article is an open access article distributed under the terms and conditions of the Creative Commons Attribution (CC BY) license (<http://creativecommons.org/licenses/by/4.0/>).